JOURNAL OF GEOPHYSICAL RESEARCH, VOL. 103, NO. B11, PAGES 26,885-26,898, NOVEMBER 10, 1998

115.

Teleseismic estimates of radiated seismic energy: The E/M_0 discriminant for tsunami earthquakes

Andrew V. Newman and Emile A. Okal

Department of Geological Sciences, Northwestern University, Evanston, Illinois

Abstract. We adapt the formalism of Boatwright and Choy for the computation of radiated seismic energy from broadband records at teleseismic distances to the real-time situation when neither the depth nor the focal geometry of the source is known accurately. The analysis of a large data set of more than 500 records from 52 large, recent earthquakes shows that this procedure yields values of the estimated energy, E^E, in good agreement with values computed from available source parameters, for example as published by the National Earthquake Information Center (NEIC), the average logarithmic residual being only 0.26 units. We analyze the energy-to-moment ratio by defining $\Theta = \log_{10}(E^E/M_0)$. For regular earthquakes, this parameter agrees well with values expected from theoretical models and from the worldwide NEIC catalogue. There is a one-to-one correspondence between values of Θ that are deficient by one full unit or more, and the so-called "tsunami earthquakes", previously identified in the literature as having exceedingly slow sources, and believed due to the presence of sedimentary structures in the fault zone. Our formalism can be applied to single-station measurements, and its coupling to automated real-time measurements of the seismic moment using the mantle magnitude M_m should significantly improve real-time tsunami warning.

1. Introduction

The purpose of this paper is to develop a measurement of the high-frequency characteristics of an earthquake source, which can be implemented in real-time for routine processing of teleseismic events. We are motivated in this endeavor by the need to recognize in real time, and hopefully through an automated algorithm, the so-called "tsunami earthquakes" [*Kanamori,* 1972], characterized by a significant deficiency of moment release at high frequencies. We wish to emphasize here several concepts, notably the difference between a tsunamigenic earthquake, which is merely an earthquake having generated an observable tsunami, and a "tsunami earthquake", defined as an event whose tsunami is significantly larger than would be expected from its seismic waves. Among the latter, *Kanamori and Kikuchi* [1993] have discussed the possible difference between overthrusting events occurring at the interplate contact (but in the presence of a weakened fault zone, thus resulting in an extremely slow rupture and a strongly anomalous earthquake source spectrum) and those events taking place at very shallow depths inside structures such as accretionary prisms (leading to enhanced tsunami generation because of the propagation of rupture through sedimentary layers to the actual seafloor [*Okal,* 1988] and of the possibility of slumping). An example of the first type is the 1992 Nicaraguan earthquake [*Kikuchi and Kanamori,* 1995], whereas the 1975 Kuriles and 1982 Tonga events could be of the second type [*Fukao,* 1979; *Lundgren et al.,* 1989]. While the presence of sedimentary structures in the rupture zone is believed to play a role for both types, significant differences exist between them. In particular, the seismic spectrum of the first type of tsunami earthquake, affected by a slower rupture, may be easier to identify by purely seismic methods, as discussed in the present paper.

Paper number 98JB02236.
0148-0227/98JB-02236$9.00

In a previous contribution, *Okal and Talandier* [1989] developed the concept of the mantle magnitude M_m, measured at a variable, but very long, period (always in excess of 50 s), and related to the physical measure of the static properties of the seismic source, namely the seismic moment M_0, through

$$M_m = \log_{10} M_0 - 20 \qquad (1)$$

where M_0 is expressed in dyn-cm. While based on rigorous theoretical foundations, M_m kept the philosophy of a magnitude scale, i.e., of a real-time, single-station, "quick and dirty" estimation of the seismic moment, not requiring the precise knowledge of such characteristics as source depth or focal mechanism. Later work showed that the measurement of M_m could be automated and led to the development of the TREMORS detection and evaluation algorithm [*Reymond et al.,* 1991], now operational at several locations around the world.

Our approach in the present work will share a very similar philosophy: We propose to implement the measurement of the seismic energy radiated by the seismic source, as detailed by *Boatwright and Choy* [1986], in the context of real-time observatory conditions, when neither the exact focal depth of the event nor its focal geometry is known accurately.

Because the calculation of energy involves the squared time series of the ground velocity, it measures the high-frequency properties of the source. By comparing the estimated energy with the seismic moment of the event, obtained in real time from measurements of the mantle magnitude M_m, we define a dimensionless parameter, $\Theta = \log_{10}(E/M_0)$, which is a powerful discriminant for any significant anomaly in the earthquake's source spectrum. This parameter can be regarded as a modern, quantified expression of the classical m_b:M_s discriminant, which has long been used to identify singular source characteristics, notably for the purpose of identifying nuclear explosions [e.g., *Marshall and Basham,* 1972].

We show that the parameter Θ easily identifies the three recent tsunami earthquakes (Nicaragua, 1992; Java, 1994;

Chimbote, Perù, 1996) through a deficiency of one unit of magnitude in Θ. Thus the implementation of its automated computation into real-time detection and quantification algorithms, of which the present paper lays the foundation, could be an important step forward in furthering realistic efforts in accurate tsunami warning.

2. Methodology

An algorithm for measuring the energy radiated by a seismic source has been given by *Boatwright and Choy* [1986]. Here, we review the principal steps of the computation. Starting with the ground motion time series $u(t)$ of the generalized P wave (the combination of direct P, pP, and sP) recorded at a teleseismic station, we first compute the energy flux ε at the station, integrated over the duration of the generalized P wave

$$\varepsilon = \rho \alpha \int_0^\infty \dot{u}^2(t)\, dt \qquad (2)$$

where ρ and α are the local density and P–wave velocity at the receiver, respectively, and the upper bound of the integral has been extrapolated to $+\infty$. In practice, it is preferable to use Parseval's theorem to evaluate (2) in the frequency domain, which allows an immediate correction for the effect of anelastic attenuation, leading to

$$\varepsilon^* = \frac{\rho \alpha}{\pi} \int_0^\infty \left| \omega \cdot u(\omega) \right|^2 \exp[\omega\, t^*(\omega)]\, d\omega \qquad (3)$$

ε^* is then scaled back to a focal sphere of unit radius, through the use of geometrical spreading, yielding

$$\varepsilon^*_{FS} = (R^P)^2\, \varepsilon^* \qquad (4)$$

where $R^P = a/g(\Delta)$, a being the radius of the Earth, and $g(\Delta)$ the familiar dimensionless geometrical spreading coefficient, given for example by *Okal* [1992]. Note that R^P is equivalent to $\mathscr{R}^P$ in the notation of *Aki and Richards* [1980, p. 99]; we assume for simplicity that the source and receiver have similar material properties; ε^*_{FS} represents the energy leaving the source in the generalized P wave per unit solid angle surrounding the generalized ray. The calculation is finalized by correcting for the appropriate radiation pattern in the direction of the station, and integrating over the focal sphere

$$E^P = 4\pi \frac{< (F^P)^2 >}{(F^{gP})^2}\, \varepsilon^*_{FS} \qquad (5)$$

where $(F^P)^2$ is the squared radiation pattern of a P wave; $< (F^P)^2 > = 4/15$ is its average over the focal sphere; and the generalized radiation coefficient is given by Equation (10) of *Boatwright and Choy* [1986]:

$$(F^{gP})^2 = (F^P)^2 + (\dot{P}\dot{P} \cdot F^{pP})^2 + \frac{2\alpha}{3\beta}\, q\, (SP^{BC} \cdot F^{sP})^2 \qquad (6)$$

In this formula, $\dot{P}\dot{P}$ is the reflection coefficient for the phase pP at the surface; SP^{BC}, the coefficient used by Boatwright and Choy, is obtained by correcting the classic reflection coefficient for displacements $\dot{S}\dot{P}$, as given for example by *Aki and Richards* [1980, p. 140], to reflect the near source expansion of the spherical S wave [*Okal,* 1992]:

$$SP^{BC} = \frac{\beta}{\alpha} \frac{\cos i_h}{\cos j_h}\, \dot{S}\dot{P} \qquad (7)$$

When the contribution of the generalized S wave is added, the total energy E^T radiated by the seismic source is computed as

$$E^T = (1+q)\, \frac{16}{5}\, \frac{(R^P)^2}{(F^{gP})^2}\, \rho\alpha \int_0^\infty \omega^2 \left| u(\omega) \right|^2 \exp[\omega\, t^*(\omega)]\, d\omega \qquad (8)$$

where $q = 15.6$ is a constant expressing the partitioning of seismic energy at the source between P and S waves [*Boatwright and Fletcher,* 1984].

In practice, there is no difficulty in implementing this algorithm, and estimates of energy release are routinely given for earthquakes with $m_b > 5.8$, as part of Preliminary Determination of Epicenters (PDE) monthly (and occasionally weekly) bulletins produced by the U.S. Geological Survey. A data set of nearly 400 events was analyzed by *Choy and Boatwright* [1995], notably with respect to the relation between radiated seismic energy and seismic moment; they obtained a value of 1.6×10^{-5} (or $10^{-4.80}$) as a least-squares fit to the ratio E/M_0 but cautioned that significant scatter existed about that value and, in particular, that strike-slip earthquakes seemed to exhibit high E/M_0 ratios. A discussion of this observation is given below.

2.1. Estimating Radiated Energy Without Knowledge of Source Parameters

In real-time observational conditions, when neither depth nor focal mechanism is known accurately, several steps in the above algorithm will be affected. Specifically, we need to replace several terms in (8) with adequate substitutes obtained from averages over representative depths and focal geometries. This approach is similar in scope and method to the development of the source correction C_S used in the computation of the mantle magnitude M_m [*Okal and Talandier,* 1989].

2.1.1. Radiation Pattern. In the absence of accurate knowledge of depth and geometry, we need to replace the equation (6) giving the generalized radiation coefficient with an adequate average value. Note that $(F^{gP})^2$ is controlled by the geometry of the source but also features a small depth dependence, through the various take-off angles of the individual rays involved. The well-known averages of the squared radiation patterns of a P wave (4/15) and an SV wave (1/5) on the focal sphere [*Aki and Richards,* 1980] are not immediately applicable, for several reasons. First, the relative orientation in space of the three rays P, pP, and sP leaving the source is not random, making it impossible, for example, for all three to simultaneously have maximum amplitude. In addition, the take-off angles (i_h and j_h) at the hypocenter are depth- and distance-dependent, as are the reflection coefficients $\dot{P}\dot{P}$ and $\dot{S}\dot{P}$. Finally, the distribution of focal mechanisms in the most active seismic belts is not random.

As a result of these complexities, the variation with focal geometry of the generalized coefficient (Equation 6) is significantly more intricate than in the case of surface waves. In particular, the separation of the surface wave spectra into their excitation and propagation parts [*Harkrider,* 1964] does not apply to body waves, and the distance dependence of $(F^{gP})^2$ must be taken into account when replacing the true correction with an average one.

2.1.1.1. The case of strike-slip earthquakes: A case of particular importance is that of earthquakes featuring (or approaching) strike-slip motion on a vertical fault ("strike-slip earthquakes"), when recorded at large distances. In that geometry, and especially for shallow sources, all three rays contributing to the generalized P wave leave the source close to the null axis, and the radiation pattern coefficients F^P, F^{pP}, and F^{sP}, as well as the reflection coefficient $\dot{S}\dot{P}$, are all very small, as is therefore the generalized radiation coefficient $(F^{gP})^2$. This well-known property was duly stressed by *Boatwright and Choy* [1986], for example in their Figure 1.

Conversely, the correction from energy flux to radiated energy (Equation 5) becomes infinite when the generalized ray approaches the direction of the null axis, and obviously decreases very rapidly in the immediate vicinity of this geometry. A significant problem then arises in instances when the assumed geometry of the ray is inadequate, for example if

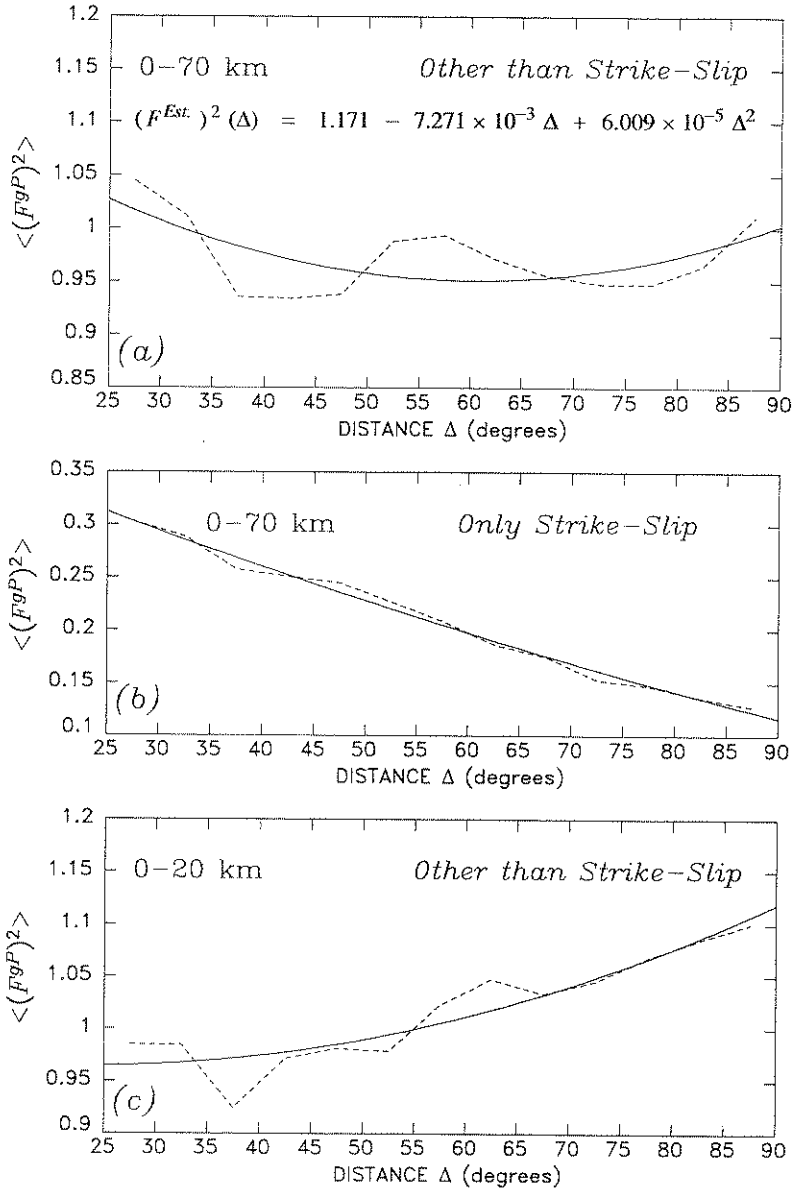

Figure 1. (a) The dashed line shows the variation, as a function of epicentral distance Δ, of the squared generalized radiation coefficient $(F^{sP})^2$, averaged over a large number of realistic source-receiver combinations (see text and Table 1 for details). The solid line represents the second-order polynomial spline (Equation 9) best fitting the dashed line. Strike-slip earthquakes are excluded. (b) Same as (a), but for strike-slip sources; note different vertical scale. (c) Same as (a), but for shallowest events.

the focal mechanism is inaccurate or in the presence of lateral heterogeneity resulting in multipathing or scattering, a ubiquitous situation at the high frequencies controlling the ground velocity spectrum. We would then expect that the use of the exact generalized radiation coefficient in (5) would result in systematic over-correction of the energy flux. Other focal geometries are much less sensitive to this problem because for them, the three coefficients F^P, F^{pP}, and F^{sP} cannot vanish (or approach zero) simultaneously; consequently, $(F^{sP})^2$ is generally not extremal in the ray's geometry, and no systematic bias is introduced by either an inaccurate focal mechanism or the presence of non-geometrical effects. We believe that the singular character of strike-slip earthquakes reported by *Choy and Boatwright* [1995] is an artifact of this effect.

Note also that *Okal and Talandier* [1989] used a very similar argument to justify using an average focal correction in the calculation of the mantle magnitude M_m, even in the vicinity of a node of radiation; they pointed out that in such a configuration, the magnitude concept, which ignores the exact focal geometry, could be a more robust measure of the true size of the event than one correcting for an expected small source excitation, but failing to account for non-geometrical effects. Similarly, magnitude measurements, such as estimates of M_s at periods of 20 s, are largely insensitive to source-receiver geometry, because of the ability of these relatively high-frequency surface waves to propagate energy off great-circle paths and to contribute seismic amplitude even at stations that are expected to be nodal. Clearly, the problem is only exacerbated when going to higher frequencies, such as the 1–Hz range typical of teleseismic P waves.

2.1.1.2. Developing an average focal correction: We proceed to obtain an average coefficient, $(F^{Est.})^2$ as a function of epicen-

tral distance as follows: We start with the full Harvard Centroid Moment Tensor (CMT) catalogue for shallow earthquakes ($h \leq 70$ km) for the years 1977–1995 (*Dziewonski et al.* [1983] and subsequent quarterly updates). As discussed above, it is expected that for strike-slip earthquakes, the computation of the generalized radiation coefficient (6) may significantly underestimate the actual energy finding its way into the seismogram; for this reason, we eliminate from the catalogue all strike-slip events, broadly defined as those for which the steepest axis of the moment tensor is the null axis. This leaves 6808 non-strike-slip events. We then use 136 stations belonging to various worldwide networks and accessible from the IRIS Data Management Center, resulting in 442,547 source-receiver combinations at distances between 25° and 90°. The average value of $(F^P)^2$ for this data set is 0.420 (significantly greater than the mathematical average of 0.267), and the average $(F^{gP})^2$ is 0.971; the difference is attributable mainly to the contribution of sP. The average $(F^{gP})^2$ is found to vary rather irregularly with distance, as shown in Figure 1, where the data set has been binned into 5° distance increments. A second-order polynomial regression through the 13 distance bins shows that the distance-dependent focal correction

$$(F^{Est.})^2(\Delta) = 1.171 - 7.271 \times 10^{-3}\Delta + 6.009 \times 10^{-5}\Delta^2 \qquad (9)$$

(Δ in degrees) best fits in a least squares sense the average squared generalized radiation coefficient for an extensive data set of source-receiver combinations representative of real-time operational geometries.

Figure 1 also shows the result of a similar investigation of 165,590 rays from 2887 strike-slip events. A significant trend with distance is present, which can be explained simply in terms of the regular steepening with distance of the rays taking off at the source and of their consequent approach of the null axis for such mechanisms. Even though its presentation is different, Figure 1 is in excellent agreement with *Boatwright and Choy*'s [1986] Figure 1, in regard to the values reached by $(F^{gP})^2$ and the relative deficiency (a factor of ~4) in the case of strike-slip earthquakes.

Finally, by restricting our experiment to 72,504 rays from 1107 events reported at depths < 20 km, we verified that source depth plays only a minor role on the best fitting parameters in (9); $(F^{Est.})^2$ would differ by at most 11% at 90°, and < 6% for $\Delta \leq 60°$. Since we are eventually concerned with interpreting the ratio of energy to seismic moment, we emphasize that these deviations represent 0.045 and 0.025 orders of magnitude, respectively, well within the precision range of any conceivable real-time measurement. Table 1 summarizes estimates of second-order polynomial splines best fitting the variation with distance of the average generalized radiation coefficient for various kinds of sources.

2.1.2. Geometrical Spreading. The geometrical spreading factor, $R^P = a/g$ in Equation (8), is a function of both receiver distance and source depth. As discussed by *Kanamori and Stewart* [1976], $g(h;\Delta)$ varies smoothly between 30° and 90°, and has very little sensitivity to depth. For the purpose of computing an estimate of the radiated energy, we use $g(15;\Delta)$ calculated at the default depth $h = 15$ km.

2.2. Other Operational Procedures.

We discuss here certain aspects of the operational procedure of calculating the estimated energy.

2.2.1. Frequency Band. It is clearly impossible to carry out the integral (3) from 0 to infinite frequency, as required by Parseval's theorem, or even in the context of discrete Fourier transforms, from the sample frequency to the Nyquist frequency. By monitoring the growth of the integral (3) with ω, we have found that in most instances, the upper bound $f_{max} = 2$ Hz ($\omega_{max} = 4\pi$ rad/s) provides an adequate estimate of the teleseismic energy. This conclusion is in agreement with *Vassiliou and Kanamori*'s [1982] observations.

Regarding the lower bound of the integral (3), we use a time window of 70 s following the arrival of direct P, a compromise between contamination of the record by later phases such as PcP and coverage of the full duration of the seismic source. Note that, in an operational procedure, the length of the time window could be refined if the mantle magnitude suggests a very large seismic moment (scaling laws would suggest a threshold of $\sim 5 \times 10^{28}$ dyn-cm [*Geller*, 1976]). There is no computational difficulty in starting the integration at the sample frequency ($f_{min} = 14$ mHz) when using modern broadband seismograms. However, when applying this technique to older, short-period instruments of the Global Digital Seismograph Network (GDSN), we found that the integration cannot be started before $f_{min} = 0.1$ Hz.

2.2.2. Q Correction. In their original paper, *Boatwright and Choy* [1986] corrected for anelastic attenuation in Equation (3) using *Der et al.*'s [1982] frequency-dependent t^* parameter (in s), $t^* = 0.8 - 0.3 \log_{10} f$ for $f \leq 1$ Hz, and $t^* = 0.8 - 0.7 \log_{10} f$ for $f \geq 1$ Hz. In their more recent paper describing the NEIC procedure, *Choy and Boatwright* [1995] used a somewhat less attenuating operator, which can be modeled as

$$\begin{aligned} t^* &= 0.9 - 0.1 \log_{10} f \qquad (f \leq 0.1 \text{ Hz}) \\ t^* &= 0.5 - 0.5 \log_{10} f \qquad (0.1 \leq f \leq 1 \text{ Hz}) \\ t^* &= 0.5 - 0.1 \log_{10} f \qquad (f \geq 1 \text{ Hz}) \end{aligned} \qquad (10)$$

Following their practice, we use Equations (10) as a worldwide average attenuation operator; more appropriate station-dependent functions $t^*(f)$ could conceivably be used at individual receivers.

Table 1. Average Values of Radiation Coefficients for CMT/IRIS Data Sets

Data Set	Number of Events	Number of Rays	$<(F^P)^2>$	$<(F^{gP})^2>$	Regression $(F^{Est.})^2 = a + b\,\Delta + c\,\Delta^2$		
					a	b	c
All shallow events	9695	608,137	0.321	0.759	1.011	-8.590×10^{-3}	6.747×10^{-5}
Non strike-slip	6808	442,547	0.420	0.971	1.171	-7.271×10^{-3}	6.009×10^{-5}
Only strike-slip	2887	165,590	0.060	0.194	0.407	-4.011×10^{-3}	8.783×10^{-6}
Shallowest (0–20 km) non-strike-slip events	1107	72,504	0.479	1.026	0.983	-1.605×10^{-3}	3.457×10^{-5}

2.2.3. Receiver Parameters and Response. We use $\rho = 3$ g/cm^3 and $\alpha = 7$ km/s as receiver parameters in Equation (8) and correct the seismic signal $s(t)$ both for instrument response I and receiver function C^P [*Okal*, 1992], the latter being itself a function of distance and (slightly) of source depth, to obtain the ground motion displacement, best expressed in the frequency domain as

$$u(\omega) = \frac{s(\omega)}{I(\omega)\ C^P(15;\Delta)} \tag{11}$$

The final result of this algorithm is an estimated value,

$$E^E = (1+q)\ \frac{16}{5}\ \frac{[a/g(15;\Delta)]^2}{(F^{Est.})^2}\ \rho\alpha\ \cdot \cdot \int_{\omega_{min}}^{\omega_{max}} \omega^2 \left|u(\omega)\right|^2 \exp[\omega t^*(\omega)]\ d\omega \tag{12}$$

of the true energy E^T that would be computed from the exact parameters $g(h;\Delta)$ and $(F^{sP})^2$. We call E^E the "estimated energy" and E^T the "corrected energy".

3. Application to a Data Set of 52 Large Earthquakes

3.1. Data Set

In this section, we apply the above formalism to a data set of large earthquakes. Keeping in mind the eventual application of our formalism to tsunami warning, we restrict our analysis to events in the oceanic environment. We initially started with the 30 shallow earthquakes since 1990 with scalar moments reported by the Harvard group as $> 10^{27}$ dyn-cm (*Dziewonski et al.* [1991] and subsequent quarterly updates), from which we deleted those events occurring on land (Iran; Luzon; Landers, California; etc.). We completed this data set by including several older and/or smaller events ($M_0 \geq 1.4 \times 10^{26}$ dyn-cm) on the rim of the Pacific and also the largest 1997 shocks. Among modern reported tsunami earthquakes, we have included Event 4 (Tonga 1982) but were unable to obtain adequate digital data for the Kuriles earthquake of June 10, 1975, studied by *Fukao* [1979]. The final data set, listed in Table 2, consists of 52 earthquakes. All source parameters are derived from the CMT catalogue. Note that Event 29 ($h = 88$ km) was retained because its bulletin depths are significantly shallower (NEIC: 21 km; ISC: 47 km).

For 42 of these events, radiated energy values have been published by the NEIC, either listed by *Choy and Boatwright* [1995], reported in the PDE monthly and weekly bulletins, or transcribed by the ISC. Unfortunately, no estimate of energy is available for Event 42, the Chimbote tsunami earthquake of February 21, 1996, presumably because its body-wave magnitude m_b falls exactly at the threshold (5.8) of study by the NEIC.

For each earthquake in our data set, we analyzed from 3 to 23 records ($25° \leq \Delta \leq 90°$); the lower number corresponds to the earlier events, for which only a few short-period GDSN channels provided adequate signal-to-noise ratios. Both the estimated and the corrected values of the energy were computed for each record and were then averaged geometrically (i.e., their logarithms averaged arithmetically) for each event. Only these average values are listed in Table 2, but the full data set for the 540 records analyzed was also kept.

3.2. Comparison with Published Values

Figure 2 compares the average estimated energy with the NEIC values for each of the 42 earthquakes. Two characteristics are immediately apparent. First, five earthquakes are given significantly lower energy estimates [by factors varying between 9 ($10^{0.96}$) and 25 ($10^{1.40}$)] than in *Choy and Boatwright*'s [1995] study: these are the three 1987–88 events in the Gulf of Alaska (Events 6, 7, and 8), the 1989 Macquarie earthquake (Event 9), and the 1994 Halmahera earthquake (Event 23). The first four were the most energetic events in *Choy and Boatwright*'s [1995] catalogue; the fifth is a relatively small earthquake ($M_0 = 3.2 \times 10^{26}$ dyn-cm), that generated a small local tsunami on the West coast of Halmahera [*Schindelé et al.*, 1995]. All five are strike-slip earthquakes.

Importantly, the values of $\Theta = \log_{10}(E^E/M_0)$ for these five events are in no way anomalous. For Events 7, 8, and 23, they are –4.83, –4.85 and –4.75, respectively, indistinguishable from the worldwide average (–4.80) reported by *Choy and Boatwright* [1995]. The ratio for Event 6 is higher by a factor of ~2, but this does not make it particularly anomalous, its Θ (–4.54) being similar to those of such non-strike-slip shocks as the 1993 Japan Sea and Guam events. Finally, the Macquarie earthquake (–5.32) is, if anything, slightly deficient with respect to *Choy and Boatwright*'s [1995] average.

Even when the corrected energies E^T are used, i.e., when the CMT radiation pattern is taken into account, the E^T/M_0 ratios for the five earthquakes do not appear particularly anomalous (Figure 3). As expected for strike-slip events, the energy E^T is ~4 times greater than E^E, but the parameters $\Theta^T = \log_{10}(E^T/M_0)$, remain in the vicinity of –4.20 (–4.7 for Macquarie), ~0.8 units below the values reported by *Choy and Boatwright* [1995]. The origin of this discrepancy probably lies in a different choice of focal mechanism, since all focal geometries used in our study are taken from the Harvard CMT files, whereas Choy and Boatwright used various sources (as is probably also the case for the energy values reported in the PDEs for events postdating their study). For example, in the case of Events 6, 7, 8, and 9, we find N–axis plunge angles of 83°, 87°, 79°, and 85°, respectively, when using the NEIC mechanisms, compared with 57°, 69°, 71°, and 67° for the CMT mechanisms. Yet, in all cases, the mechanisms (NEIC or CMT) would be described as "strike-slip" based on the N axis being the most steeply dipping of the three principal axes.

As explained in Section 2.1.1, only steeply dipping N axes allow all three coefficients F^P, F^{pP}, and F^{sP} to become simultaneously very small for distant stations. In addition, in the probable presence of lateral heterogeneity resulting in multipathing, the assumption that a station is quasi-nodal for all three components of the generalized P wave may not be justified, and may lead to significant over-correction and hence to artificially enhanced E/M_0 ratios. Because high-frequency energy will find its way into the seismogram along non geometrical paths, our method, which uses the average correction $(F^{Est.})^2$, actually guards against this artifact.

Finally, one could ask whether this reported trend, for NEIC solutions of strike-slip earthquakes to have steeper N axes than their Harvard CMT counterparts, is fortuitous or systematic. To answer this intriguing question would require using a much larger data set and clearly transcends the scope of this paper.

The second characteristic of Figure 2 is that our values are generally larger than their NEIC counterparts. The average value of the residual $r = E^E - E^{NEIC}$ is $\bar{r} = 0.09$ logarithmic units, but $\bar{r}$ grows to 0.26 if the five anomalous strike-slip events are excluded. This means that our energy estimates are on the average 1.82 times greater than the NEIC's. The origin of this bias is not clear, but it may be due to subtle differences in computational algorithms between the works of *Boatwright and Choy* [1986], *Choy and Boatwright* [1995], and the present study. However, this bias will not affect the conclusions of this

Table 2. Events Used in This Study and Resulting Estimates of Energy

Event	Date (Julian Day)	Time	Epicenter	CMT Solution			E^{NEIC},	E^E,	E^T,	r	Θ	Θ^T
		UT	°N; °E	Depth, km	ϕ, δ, λ, deg	M_0, 10^{27} dyn-cm	10^{23} erg	10^{23} erg	10^{23} erg			
1	Apr. 06, 1982 (096)	1956	13.79; -91.95	43	290, 27, 74	0.14		0.008	0.006		-5.23	-5.34
2	June 19, 1982 (170)	0621	12.65; -88.97	52	102, 25, 254	1.05		0.032	0.071		-5.52	-5.17
3	Nov. 19, 1982 (323)	0427	-10.44; -74.95	10	0, 34, 116	0.11		0.031	0.023		-4.54	-4.66
→ 4	Dec. 19, 1982 (353)	1743	-24.31; -175.10	29	198, 22, 101	2.00		0.035	0.037		-5.76	-5.73
5	Dec. 02, 1983 (336)	0309	13.86; -92.20	31	296, 19, 89	0.37		0.021	0.023		-5.25	-5.21
6	Nov. 17, 1987 (321)	0846	58.87; -143.62	15	262, 57, 354	0.66	2.6	0.190	0.469	-1.136	-4.54	-4.15
7	Nov. 30, 1987 (334)	1923	58.17; -142.04	15	355, 70, 188	7.30	27.	1.080	4.300	-1.398	-4.83	-4.23
8	Mar. 06, 1988 (066)	2235	57.37; -143.53	15	182, 75, 192	4.90	9.7	0.694	3.130	-1.145	-4.85	-4.19
9	May 23, 1989 (143)	1054	-52.15; 160.41	15	34, 69, 170	14.00	9.7	0.673	2.880	-1.159	-5.32	-4.69
10	Mar. 03, 1990 (062)	1216	-22.05; 175.35	25	228, 68, 4	3.00	0.17	0.140	0.682	-0.084	-5.33	-4.64
11	Mar. 25, 1990 (084)	1322	9.95; -84.58	18	303, 11, 104	1.10	0.022	0.078	0.053	0.551	-5.15	-5.32
12	Apr. 03, 1990 (093)	2257	11.24; -86.64	32	310, 19, 105	0.18	0.0034	0.010	0.008	0.468	-5.26	-5.35
13	Apr. 05, 1990 (095)	2112	15.57; 148.08	15	185, 31, 252	1.60	0.44	1.120	1.080	0.406	-4.15	-4.17
14	Apr. 18, 1990 (108)	1339	1.31; 123.35	33	112, 31, 122	3.30	0.14	0.251	0.349	0.254	-5.12	-4.98
15	Apr. 22, 1991 (112)	2156	10.10; -82.77	15	103, 25, 58	3.30	0.32	0.102	0.162	-0.497	-5.51	-5.31
16	June 20, 1991 (171)	0518	1.04; 123.23	15	109, 7, 102	2.30	0.03	0.101	0.106	0.527	-5.36	-5.34
17	Dec. 22, 1991 (356)	0843	45.58; 151.55	31	226, 16, 99	2.80	0.051	0.089	0.113	0.239	-5.50	-5.39
†18	Sep. 02, 1992 (246)	0015	11.20; -87.81	15	303, 12, 91	3.40	0.026	0.017	0.025	-0.182	-6.30†	-6.13†
19	Dec. 12, 1992 (347)	0529	-8.34; 122.49	20	80, 40, 95	5.10	0.66	1.230	1.540	0.270	-4.62	-4.52
20	June 08, 1993 (159)	1303	51.36; 158.75	46	207, 29, 79	2.00	0.025	0.079	0.068	0.498	-5.41	-5.47
21	July 12, 1993 (193)	1317	42.71; 139.28	16	0, 35, 91	4.70	0.87	1.330	2.370	0.184	-4.55	-4.30
22	Aug. 08, 1993 (220)	0834	13.06; 145.31	59	312, 18, 147	5.20	0.68	1.680	1.340	0.393	-4.49	-4.59
23	Jan. 21, 1994 (021)	0224	1.20; 127.80	15	83, 66, 186	0.32	0.51	0.056	0.198	-0.956	-4.75	-4.21
†24	June 02, 1994 (153)	1817	-11.03; 113.04	15	278, 7, 89	5.30	0.012	0.052	0.053	0.633	-6.01†	-6.00†
25	Oct. 04, 1994 (277)	1322	43.60; 147.63	68	158, 41, 24	30.00	11.	13.600	23.200	0.092	-4.34	-4.11
26	Dec. 28, 1994 (362)	1219	40.56; 142.99	28	179, 12, 67	4.90	0.45	0.342	0.457	-0.119	-5.16	-5.03
27	Feb. 05, 1995 (036)	2251	-37.61; 179.40	15	35, 32, 270	0.58	0.11	0.226	0.237	0.313	-4.41	-4.39
28	Mar. 19, 1995 (078)	2353	-4.18; 135.10	19	257, 80, 356	0.22		0.015	0.070		-5.18	-4.50
29	Apr. 07, 1995 (097)	2206	-15.37; -173.15	88	188, 18, 159	1.30	0.54	0.748	1.100	0.142	-4.24	-4.07
30	May 16, 1995 (136)	2012	-23.05; 170.00	25	280, 35, 261	3.90	0.88	1.680	1.450	0.281	-4.37	-4.43
31	July 03, 1995 (184)	1950	-29.13; -177.22	45	197, 28, 95	0.62	0.035	0.086	0.076	0.390	-4.86	-4.91
32	July 30, 1995 (211)	0511	-24.17; -70.74	29	354, 22, 87	12.00	0.55	0.399	0.659	-0.139	-5.48	-5.26
33	Aug. 16, 1995 (228)	1027	-5.51; 153.64	46	136, 42, 87	4.60	0.20	0.385	0.377	0.284	-5.08	-5.09
34	Sep. 14, 1995 (257)	1404	16.73; -98.54	22	289, 15, 85	1.30	0.14	0.248	0.270	0.248	-4.72	-4.68
35	Oct. 03, 1995 (276)	0151	-2.55; -77.53	25	234, 39, 120	0.39	0.05	0.066	0.072	0.122	-4.77	-4.73
36	Oct. 09, 1995 (282)	1535	19.34; -104.80	15	302, 9, 92	11.50	0.20	0.274	0.335	0.137	-5.62	-5.54
37	Oct. 18, 1995 (291)	1037	28.06; 130.18	18	1, 28, 242	0.57	0.05	0.155	0.257	0.491	-4.57	-4.35
38	Dec. 03, 1995 (337)	1801	44.82; 150.17	26	225, 12, 95	8.20	0.28	0.487	1.210	0.240	-5.23	-4.83
39	Jan. 01, 1996 (001)	0805	0.74; 119.93	15	36, 6, 54	7.80	0.28	1.230	0.773	0.643	-4.80	-5.00
40	Feb. 07, 1996 (038)	2136	45.29; 150.45	49	235, 28, 113	0.64	0.025	0.057	0.054	0.360	-5.05	-5.08
41	Feb. 17, 1996 (048)	0559	-0.67; 136.62	15	103, 11, 69	24.00	0.77	0.913	1.610	0.074	-5.42	-5.17
†42	Feb. 21, 1996 (052)	1251	-9.95; -80.23	15	335, 14, 88	2.20		0.025	0.042		-5.94†	-5.72†
43	Apr. 29, 1996 (120)	1440	-6.65; 155.07	54	138, 45, 99	0.76	0.051	0.139	0.139	0.435	-4.74	-4.74
44	June 10, 1996 (162)	0403	51.10; -177.41	29	248, 17, 84	8.10	0.28	0.547	0.739	0.291	-5.17	-5.04
45	June 10, 1996 (162)	1524	51.38; -176.49	36	258, 25, 105	0.85	0.05	0.118	0.146	0.373	-4.86	-4.77
46	June 11, 1996 (163)	1822	12.74; 125.41	28	144, 23, 60	0.49	0.017	0.031	0.054	0.262	-5.20	-4.96
47	June 21, 1996 (173)	1357	51.49; 159.72	24	211, 25, 83	0.15	0.011	0.011	0.013	-0.016	-5.15	-5.06
48	July 22, 1996 (204)	1419	1.34; 120.65	28	57, 13, 61	0.38		0.027	0.025		-5.15	-5.19
49	Nov. 12, 1996 (317)	1659	-15.04; -75.37	37	312, 33, 52	4.40		0.362	0.555		-5.08	-4.90
50	Apr. 21, 1997 (111)	1202	-13.33; 166.29	37	301, 39, 40	4.40	0.32	0.989	1.620	0.490	-4.65	-4.43
51	July 19, 1997 (200)	1422	15.73; -98.25	15	282, 14, 78	0.12	0.0022	0.007	0.005	0.488	-5.24	-5.35
52	Dec. 05, 1997 (339)	1126	54.08; 162.29	41	198, 22, 68	6.77		0.281	0.301		-5.38	-5.35

† The daggers flag the three tsunami earthquakes discussed in detail in the text.

→ The arrow flags the 1982 Tonga event, described as a tsunami earthquake by *Talandier and Okal* [1989].

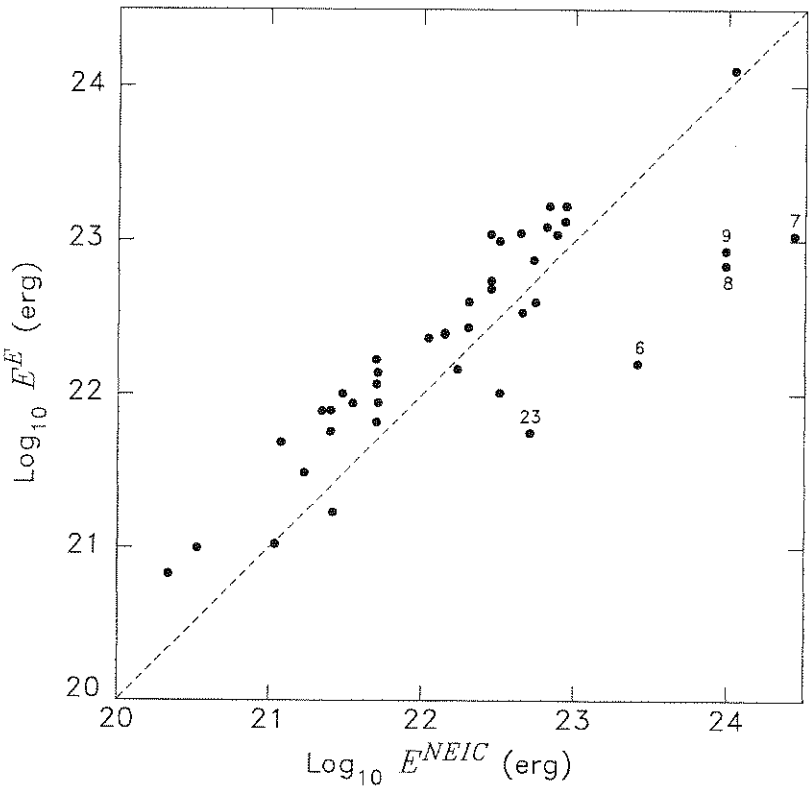

Figure 2. Values of estimated energy E^E versus published values E^{NEIC} for the 42 earthquakes common to both data sets. Events showing a deficiency in E^E are discussed in the text and identified by their numbers, which refer to Table 2.

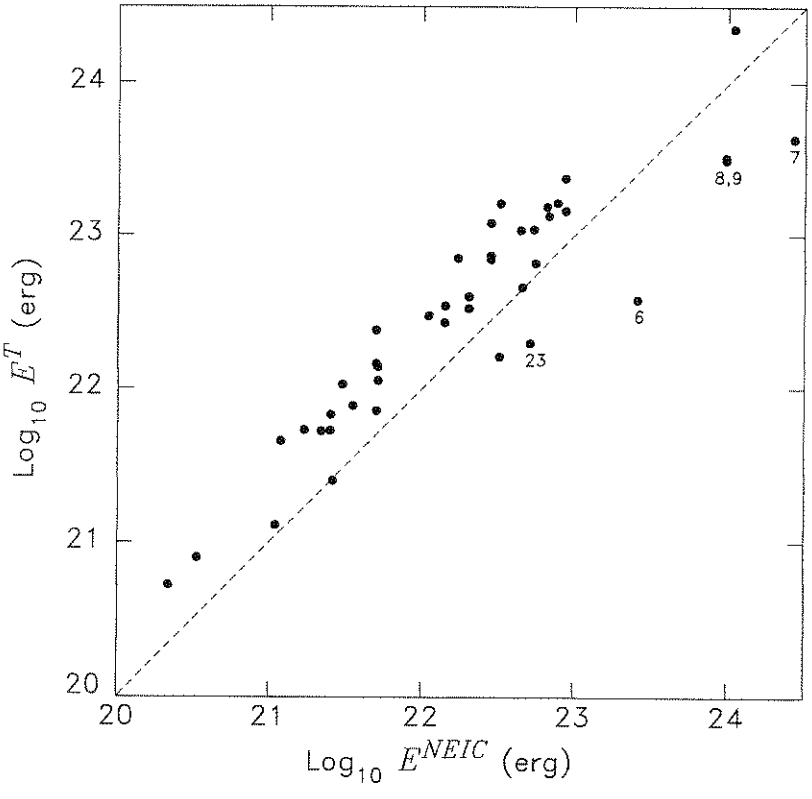

Figure 3. Same as Figure 2, for the values E^T, corrected for focal geometry. Events 8 and 9 plot on top of each other.

paper, which are based on direct comparison of estimated energies of individual earthquakes in our data set, all of which were obtained in a coherent, homogeneous fashion.

3.3. Energy-to-Moment Ratio and Discriminant Θ.

3.3.1. Background. The ratio of energy to moment has long been of interest to seismologists since this dimensionless quantity is related to the strains involved during the earthquake rupture. It has often been interpreted in terms of an apparent stress, $\sigma_a = \eta\,\bar{\sigma} = \mu\,E/M_0$ [e.g., *Kanamori and Anderson,* 1975]. In turn, and under the condition that the final stress on the fault, upon cessation of slip, has its dynamic frictional value [*Orowan,* 1960], the ratio E/M_0 can be interpreted in terms of the stress drop involved in the event by simply putting $\Delta\sigma = 2\,\sigma_a$. Consequently, energy-to-moment ratios have been used to evaluate both stress drops and ambient stress levels for various categories of earthquakes [e.g., *Wyss,* 1970; *Choy and Boatwright,* 1995]. However, this requires a model of evolution of the stress on the fault during rupture, and the a priori knowledge of the rigidity μ in the neighborhood of the source, which may be inappropriate if the rupture involves material with weak mechanical properties, such as sediments, precisely thought to play an important role in the genesis of tsunami earthquakes [*Fukao,* 1979; *Okal,* 1988; *Kanamori and Kikuchi,* 1993; *Polet and Kanamori,* 1997].

On the other hand, and following *Vassiliou and Kanamori* [1982], one can interpret the ratio E/M_0 using a more descriptive, kinematic approach that simply assumes a trapezoidal source time function of duration T_0 with rise and fall times $x\,T_0$. Vassiliou and Kanamori showed that the radiated energy E is proportional to M_0^2/T_0^3:

$$E = \left[\frac{1}{15\pi\rho\alpha^5} + \frac{1}{10\pi\rho\beta^5}\right] \frac{2}{x(1-x)^2} \frac{M_0^2}{T_0^3} \qquad (13)$$

This expression can be further transformed by writing $M_0 = \mu\,L\,W\,D$ as a function of the dislocation slip D, fault length L, and width W and introducing the rupture velocity V_R, which leads to

$$\frac{E}{M_0} = \frac{\left[1 + \frac{2}{3}\frac{\beta^5}{\alpha^5}\right]}{5\pi\,x(1-x)^2} \left[\frac{L}{T_0\,V_R}\right]^3 \frac{V_R^3}{\beta^3} \frac{W^2}{L^2} \frac{D}{W} \qquad (14)$$

The ratio E/M_0 is thus controlled by five dimensionless factors, which can be reasonably assessed on the basis of various scaling arguments [e.g., *Geller,* 1976].

1. *Vassiliou and Kanamori* [1982] argue that for most values of x between 0.1 and 0.5, $1/[x(1-x)^2]$ can be taken as ~7.5, so that for a Poisson solid the first factor is ~0.5 .

2. The second factor expresses the directivity of rupture: It will be 1 for unilateral rupture but could increase to as much as $2^3 (= 8)$ for a symmetric bilateral rupture.

3. The third factor expresses the slowness of rupture. For a regular or fast event, it can be taken as $0.8^3 (= 0.5)$, but could be as low as $0.3^3 (= 0.03)$ for a rupture slowed by sedimentary material (e.g., $V_R = 1$ km/s in otherwise crustal material, as suggested for Event 18 [*Kikuchi and Kanamori,* 1995]).

4. The fourth factor is the square of the aspect ratio of the faulting area. In most regular geometries, it would be $(1/2)^2 (= 0.25)$, but could be significantly smaller for ribbon-like ruptures on strike-slip faults.

5. Finally, and assuming the geometry of the W-model [*Scholz,* 1982], the fifth factor is the maximum strain at which the fault ruptures, ε_{rupt}. On the other hand, assuming an L-model, we would replace the last two factors with $(W/L)(D/L) = (W/L)\,\varepsilon_{rupt}$.

Thus for a regular or fast earthquake with unilateral rupture, we expect E/M_0 to be 2^{-4} times ε_{rupt}, or $E/M_0 = 1.25\times10^{-5} = 10^{-4.90}$ for $\varepsilon_{rupt} = 2\times10^{-4}$, in excellent agreement with both the value best fitting *Choy and Boatwright*'s [1995] data set ($10^{-4.80}$) and our own results ($10^{-4.98}$ excluding the four tsunami earthquakes; see Section 3.3.2). Using slightly different scaling models (e.g., $T_0 = \sqrt{S}/\beta$), *Vassiliou and Kanamori* [1982] proposed $E/M_0 = 4.6\times10^{-5} = 10^{-4.33}$.

When source conditions vary, and scaling arguments no longer hold, the ratio E/M_0 is expected to vary significantly. Each of the five factors listed above (with the probable exception of the first) could have a substantial effect, and it may be difficult to interpret an observed value of E/M_0 directly in terms of a single physical parameter such as apparent stress σ_a or stress drop $\Delta\sigma$. With this remark in mind, we note that in real-time operational conditions, such parameters as the aspect ratio of the faulting area (best obtained by precise mapping of aftershocks) will not be constrained. Consequently, in the present study, we purposely chose an empirical approach and will not seek to further interpret Θ in terms of static or dynamic stress parameters such as σ_a and $\Delta\sigma$.

3.3.2. Results. Figure 4 plots our estimated values E^E as a function of published CMT moments M_0. In this logarithmic plot, the diagonal lines map constant values of Θ. The average value of Θ for the 52 events in the data set is –5.06, and –4.98 if the four tsunami earthquakes (see Section 3.3.3 below) are excluded. The latter is 0.18 units below the least squares best-fitting value proposed by *Choy and Boatwright* [1995]. This apparent contradiction of our previous observation, that E^E values for individual earthquakes were larger than the NEIC values, stems from the fact that the average value (–4.80) derived by *Choy and Boatwright* [1995] relates to their full data set, including a large number of strike-slip earthquakes for which they found high E/M_0 ratios, whereas our data set consists mainly of thrust fault geometries.

For the large majority of earthquakes in our data set ("the mainstream population") Θ falls between –4.50 and –5.62 . This width of about 1.1 unit of magnitude compares favorably with the scatter reported by *Choy and Boatwright* [1995], although their data set was much larger and more heterogeneous than ours. Events with greater energies ($\Theta > -4.5$) are either shallow normal-faulting earthquakes (Events 13, 27, and 30), for which Choy and Boatwright did report a slight tendency towards higher E/M_0 values, or anomalously deep events (Events 22 (Guam, 1993), 25 (Kuriles, 1994), and 29). In particular, it is worth noting that three recent strong tsunamigenic earthquakes (Events 19 (Flores, 1992); 21 (Japan Sea, 1993); and 25 (Kuriles, 1994)) all have high Θ ratios.

3.3.3. The Case of the Recent Tsunami Earthquakes. We now turn our attention to events with the lowest values of E^E/M_0, which we examine in order of increasing Θ.

First, three earthquakes, emphasized with circled symbols on Figure 4 and flagged by daggers (†) in Table 2, exhibit a significant deficiency in energy relative to M_0: Events 18 (Nicaragua, 1992), 24 (Java, 1994), and 42 (Perù, 1996). Their respective Θ values, –6.30, –6.01, and –5.94, are 1.50, 1.21 and 1.14 magnitude units below *Choy and Boatwright*'s [1995] best-fitting average. All three have been described as tsunami earthquakes in the literature [e.g., *Kikuchi and Kanamori,* 1995; *Tsuji et al.,* 1995; *Tanioka et al.,* 1996]. They were characterized by significant discrepancies between their felt intensities (in all three instances, some residents on the coasts did not even feel them) and the impact of the resulting tsunamis even at transoceanic distances (significant damage was inflicted on the Australian coast from the Java event and a boat was slammed against the bottom of a harbor in the Marquesas following the Peruvian event).

The earthquake with the next lowest value of Θ (–5.76) is Event 4, the 1982 Tonga earthquake (flagged by an arrow in

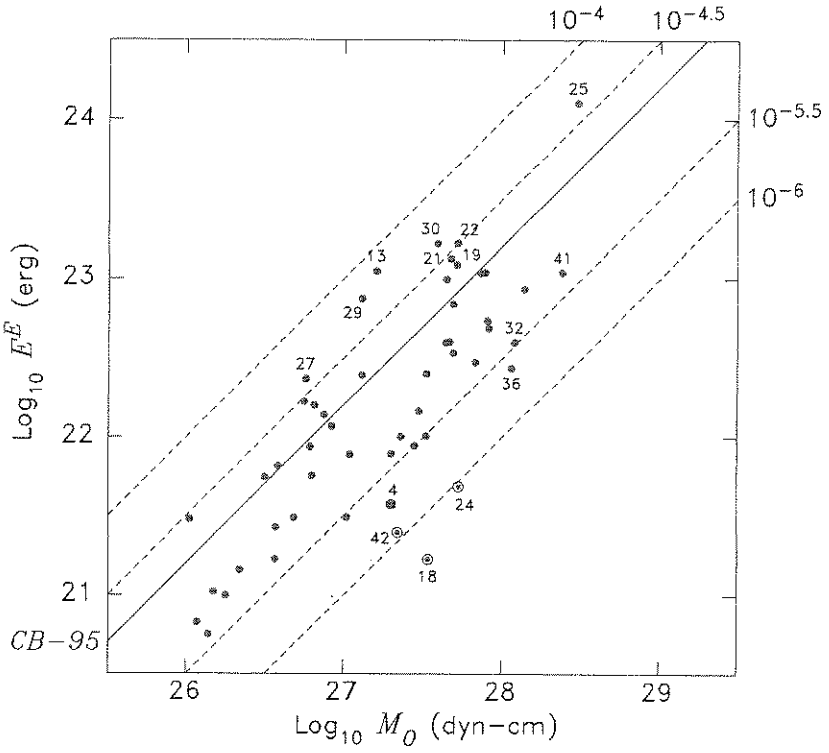

Figure 4. Estimated energy E^E versus seismic moment M_0 for the 52 earthquakes in our data set. Diagonal lines correspond to constant values of E^E/M_0. The solid diagonal (labeled *CB-95*) is for the best fitting value obtained by *Choy and Boatwright* [1995]. Significant earthquakes described in the text are identified by their numbers, in Table 2. The three recent tsunami earthquakes are shown with circled points. The 1982 Tonga tsunami earthquake (Event 4) is shown with an enlarged solid symbol.

Table 2). It was described as anomalous by *Talandier and Okal* [1989], who did label it a tsunami earthquake on account of the amplitude of its tsunami in Papeete harbor; *Schindelé et al.* [1995] also noted a modest m_b:M_0 discrepancy for this shock. *Lundgren et al.* [1989] modeled both its teleseismic body waves and the amplitude of its tsunami in Papeete using a shallow rupture of relatively short duration but reaching the ocean floor through a dipping layer of sediments. The slowing of the near-source reverberations in the sediments results in an increase in the duration of the signal, which in turns could explain a weakening of the E/M_0 ratio. We conclude that the parameter Θ adequately expresses the character of intermediate slowness of this earthquake.

With the next event ($\Theta = -5.62$) we enter the mainstream group, whose Θ values range from –4.5 to –5.62 . Incidentally, this earthquake (Event 36, Mexico, October 9, 1995) did raise a locally destructive tsunami, and its rupture velocity of only 2.8 km/s [*Courboulex et al.*, 1997] is somewhat slower than the more standard values of 3–3.5 km/s characteristic of most large interplate thrust shocks, so that it could be argued that the event is of intermediate slowness. However, it is important to realize that from there on, the population of earthquakes in our data set becomes a continuous function of growing Θ, whereas a natural break separates the three recent tsunami earthquakes (Events 18, 24, and 42), with Event 4 featuring an intermediate behavior. This is in contrast to the high-Θ end of the population, where the threshold (–4.5) used to identify the six earthquakes with highest energy-to-moment ratios described above was largely arbitrary.

Finally, it is interesting to discuss our results for other, large, tsunamigenic earthquakes in our data set. We obtain $\Theta = -5.48$ for Event 32 (the Antofagasta, Chile, earthquake of July 30, 1995), which puts it toward the lower bound of the mainstream group. This is in good agreement with its reported low M_s value and is explained by a relatively complex rupture lasting upwards of 65 s [*Ruegg et al.*, 1996]. The resulting tsunami was particularly destructive in the Marquesas Islands, owing to the resonance of local bays [*Guibourg et al.*, 1997].

We find very similar results ($\Theta = -5.42$) in the case of Event 41 (Biak, Indonesia, February 17, 1996). This is, once again, in agreement with a relatively long rupture lasting 60 s [*Dziewonski et al.*, 1997], although no systematic discrepancy was reported between that event's various magnitude estimates. Its tsunami was locally destructive.

In conclusion, the parameter Θ is an accurate descriptor of the spectral content of a large earthquake: Tsunami earthquakes involving very slow rupture along the fault and a prolonged source are characterized by values of Θ a full unit lower than average. On the other hand, no regular tsunamigenic earthquake features such deficient values of Θ.

3.4. Single-station Measurements

The above analysis of the energy-to-moment ratios of large oceanic earthquakes relied on the compilation, for each event, of the largest accessible data set of digital records at teleseismic distances. Motivated by the ultimate goal of implementing the measurement of energy into the TREMORS algorithm, which would allow the real-time, automated identification of tsunami earthquakes, we will now assess the feasibility of single-station computations of the estimated energy and hence of the discriminant Θ.

For each of the three tsunami earthquakes, we computed the magnitude M_m [*Okal and Talandier*, 1989; *Reymond et al.*, 1991] from the first passage of Rayleigh waves on very-long-

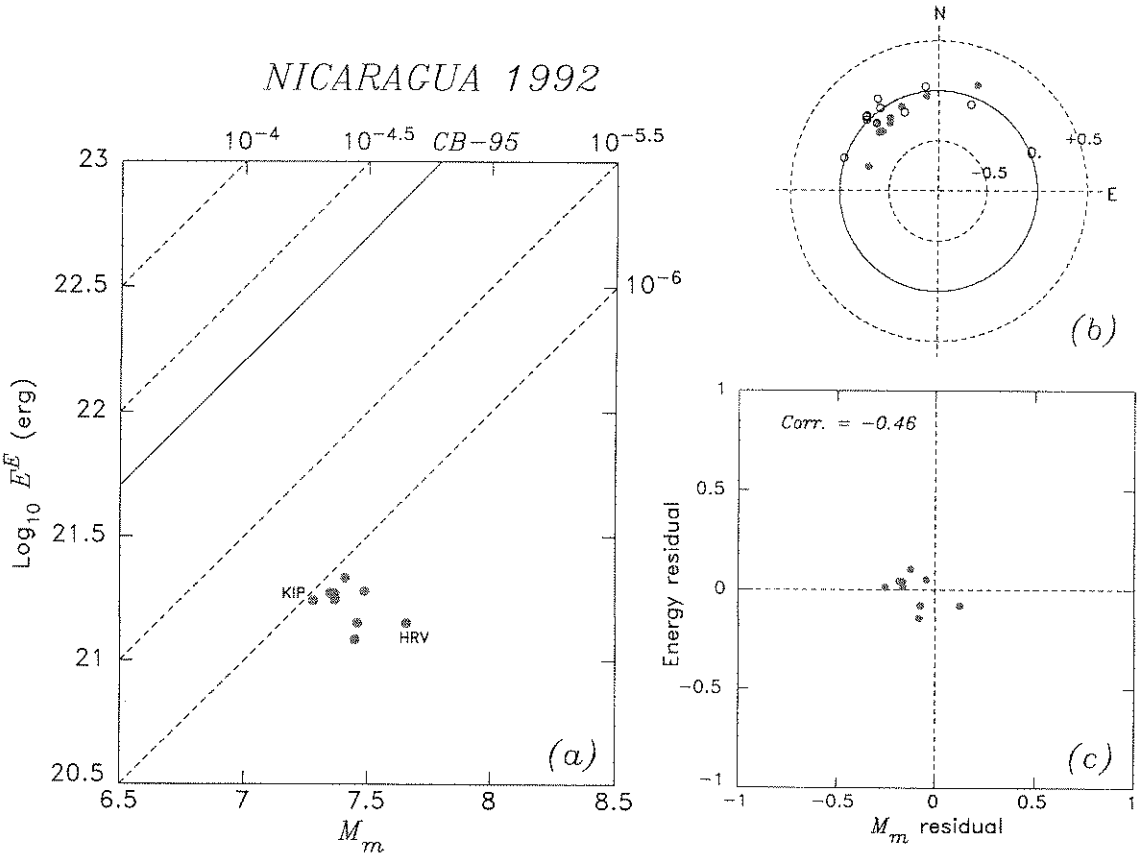

Figure 5. (a) Single-station estimates of the radiated energy E^E versus mantle magnitude M_m measured at 10 stations for the 1992 Nicaraguan tsunami earthquake (Event 18). Diagonal lines for Θ^{SS} as in Figure 4. Stations with extreme values for Θ^{SS} are identified by code. (b) Repartition of scatter in values of M_m (solid symbols) and E^E (open symbols) as a function of azimuth from epicenter; see text for details. (c) Correlation between M_m and E^E residuals.

period (VHZ) channels, at the same stations where the energy measurements were made. In this fashion, we obtained a set of single-station (SS) estimates of the parameter Θ^{SS}, now defined from single-station measurements as

$$\Theta^{SS} = \log_{10} E^E - M_m - 20 \qquad (15)$$

For the purpose of this computation, and following the automated operational procedures of the TREMORS system [*Talandier and Okal,* 1989], we retain the largest value of M_m computed in the period range 50–300 s. The resulting values of Θ^{SS} are listed in Table 3 and presented on Figures 5, 6, and 7. Figures 5a, 6a, and 7a are conceptually similar to Figure 4; in particular, the diagonal lines identify the same values of the energy-to-moment ratio, Θ^{SS}. Figures 5b, 6b, and 7b, on the other hand, examine the scatter in M_m and E^E as a function of station azimuth, as seen from the epicenter. The circles correspond to constant values of residuals, defined as follows. For moment estimates, we plot $M_m - \log_{10} M_0 - 20$, where M_0 is the CMT value listed in Table 2 (solid symbols). For energy estimates (open symbols), we plot the difference between the single-station value of $\log_{10} E^E$ and the value averaged over all stations, as listed in Table 2 and used in Figures 2 and 4. A good correlation between these residuals, as in the case of the Peruvian event, probably reflects a similar azimuthal variation of body- and surface-wave radiation patterns in the geometry of the event. Finally, Figures 5c, 6c, and 7c explore the statistical correlation between the two populations of residuals.

3.4.1. Nicaragua, 1992 (Figure 5). For this event, the scatter in individual values of both M_m and E^E is very small, and as such, the correlation coefficient is not meaningful. The parameter Θ^{SS} varies from -6.04 at Kipapa (KIP) to –6.51 at Harvard (HRV), with an average one-station value of –6.19. The most important aspect of this result is that the exceptional character of the event as being deficient at high frequencies is readily observed at all stations analyzed. Even KIP, with the highest value of Θ, exhibits a deficiency of 1.24 units with respect to *Choy and Boatwright*'s [1995] average value. The negative correlation coefficient between moment and energy residuals is actually a reflection of the small values of either population of residuals.

3.4.2. Peru, 1996 (Figure 6). In this case, the values of M_m and E^E are more scattered. There is, however, a remarkable correlation between the two sets of measurements (the correlation coefficient stands at 0.80), resulting in Θ values contained between –5.51 at Hockley (HKT), and –6.22 (at Standing Stone). In other words, since moment and energy residuals vary in the same direction among stations, the measurements of Θ^{SS} are robust. Except for HKT, all North American stations recognize the event as very slow (with Θ^{SS} about –6.0 or less). The two Pacific stations, in lobes of both P and Rayleigh excitation, give slightly higher values, but these are still 0.9 units lower than the *Choy and Boatwright* [1995] average.

3.4.3. Java, 1994 (Figure 7). This data set is by far the most scattered, Despite an apparently good correlation coefficient (0.74) for the residuals, the scatter in E^E is larger

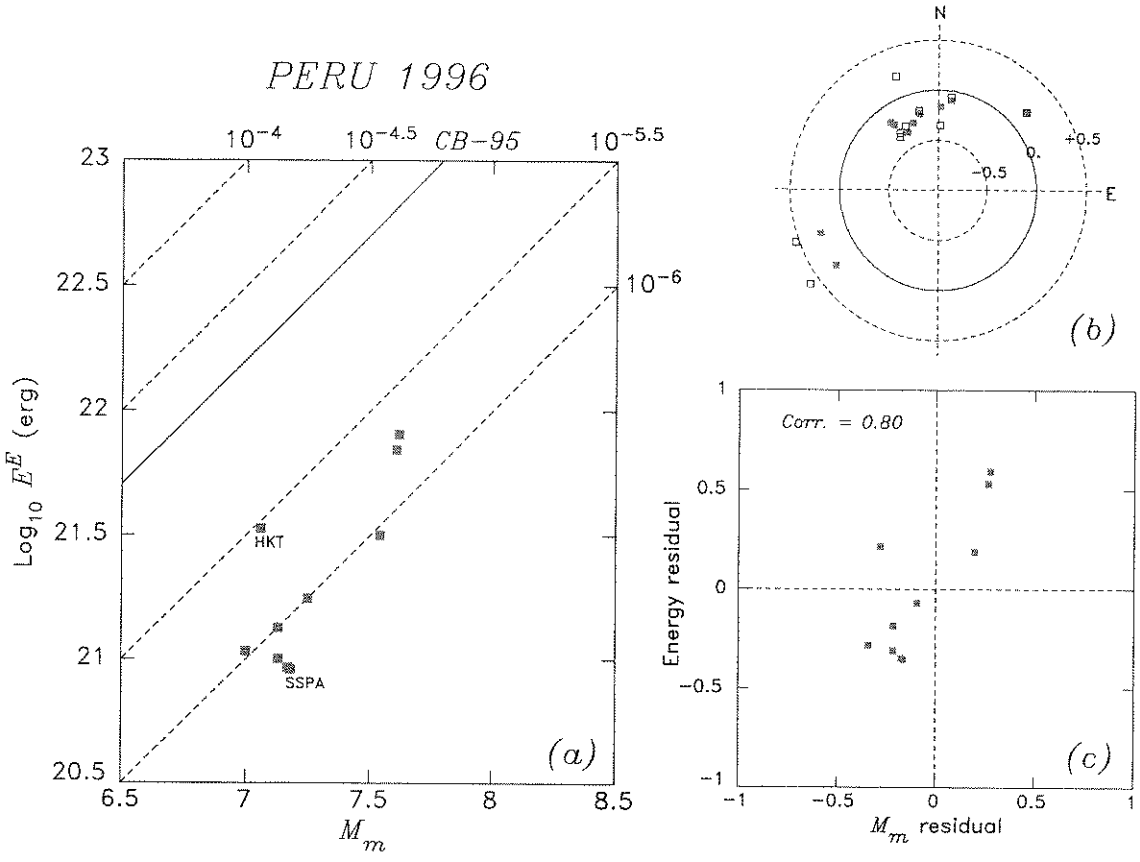

Figure 6. Same as Figure 5 at 10 stations for the 1996 Peruvian tsunami earthquake (Event 42).

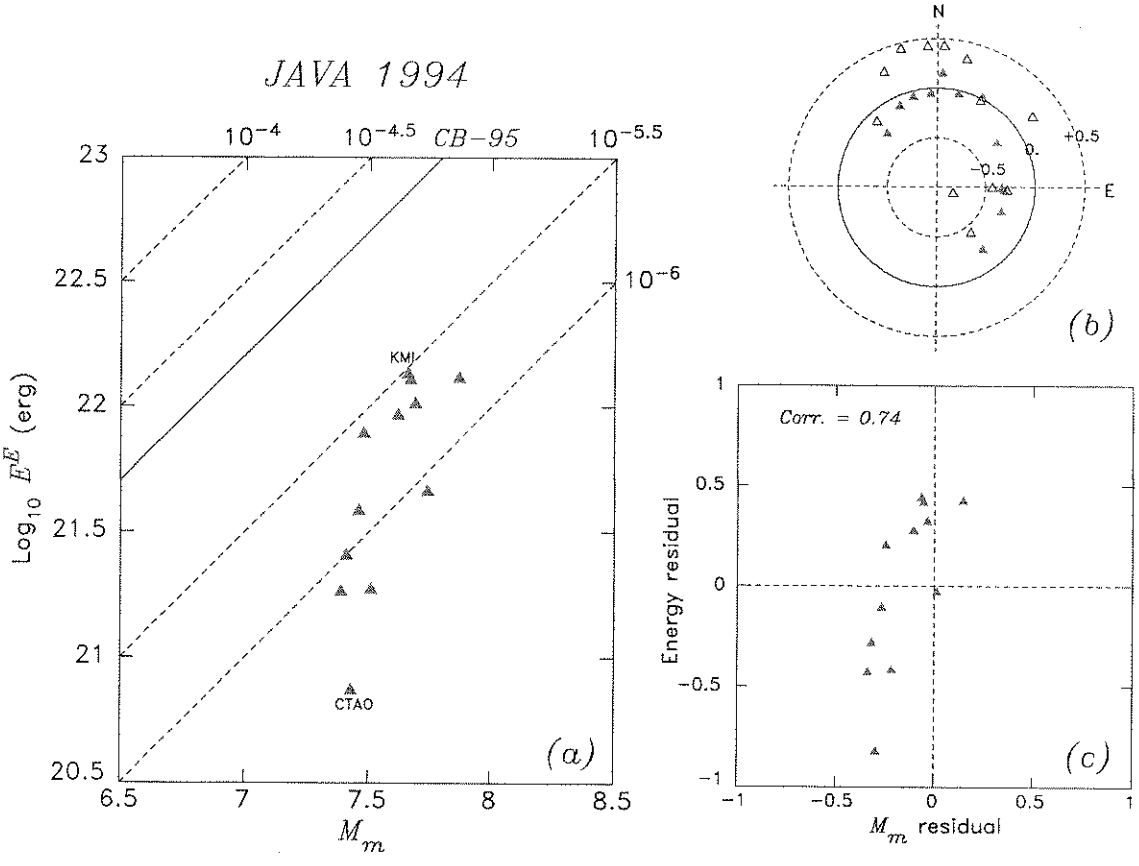

Figure 7. Same as Figure 5 at 12 stations for the 1994 Java tsunami earthquake (Event 24).

Table 3. Single-Station Measurements

Station Code	Distance, deg	Azimuth, deg	M_m	$\log_{10} E^E$, erg	Θ^{SS}
		Event 18; Nicaragua, 1992			
HRV	33.64	21	7.66	21.15	–6.51
KIP	67.93	289	7.28	21.24	–6.04
PFO	34.39	314	7.37	21.25	–6.12
ISA	36.89	315	7.37	21.27	–6.10
GSC	35.56	316	7.35	21.27	–6.08
CMB	39.46	317	7.46	21.15	–6.31
COR	44.96	324	7.37	21.25	–6.12
ANMO	28.94	326	7.41	21.33	–6.08
COL	67.11	336	7.45	21.09	–6.36
CCM	26.49	353	7.49	21.28	–6.21
		Event 24; Java, 1994			
BJT	50.46	3	7.87	22.11	–5.76
TATO	36.34	13	7.69	22.01	–5.68
PET	74.42	27	7.74	21.66	–6.08
GUMO	39.82	54	7.48	21.89	–5.59
PMG	33.81	91	7.39	21.26	–6.13
HNR	46.38	93	7.41	21.41	–6.00
CTAO	33.56	111	7.43	20.87	–6.56
TAU	44.12	143	7.51	21.27	–6.24
ABKT	70.28	317	7.46	21.58	–5.88
CHTO	32.22	335	7.62	21.97	–5.65
KMI	36.83	345	7.66	22.13	–5.53
ENH	40.76	356	7.67	22.11	–5.56
		Event 42; Peru, 1996			
SSPA	50.13	2	7.18	20.96	–6.22
HRV	52.49	8	7.25	21.25	–6.00
PAB	84.92	49	7.54	21.50	–6.04
RPN	33.07	234	7.62	21.91	–5.71
RAR	77.49	250	7.61	21.85	–5.76
CMB	60.88	324	7.17	20.97	–6.20
TUC	51.32	326	7.13	21.00	–6.13
ANMO	51.18	332	7.00	21.03	–5.97
HKT	42.43	339	7.06	21.53	–5.53
FFC	66.90	346	7.13	21.13	–6.00
		Event 19; Flores Sea, 1992			
CTAO	26.23	119	8.07	23.49	–4.58
SNZO	56.84	134	8.13	23.20	–4.93
LSA	48.23	323	8.10	23.22	–4.88
AAK	66.82	324	8.06	22.75	–5.31
KMI	38.37	331	8.25	23.29	–4.96

than in M_m values. In a systematic azimuthal pattern, Asian stations to the North overestimate E^E, relative to Australian and Pacific stations to the Southeast. This effect is certainly due in part to the focal geometry but could also reflect the geometry of the rupture propagation on what was documented to be a strongly dipping ocean floor [*Tanioka and Satake,* 1996].

Unfortunately, in the case of the 1982 Tonga earthquake (Event 4), we could not find suitable very-long-period records (VHZ channels) at the same stations (ANMO, CTAO, JAS, and LON) whose short-period records were used to compute E^E; consequently, we could not process the event in the same fashion as the three recent tsunami earthquakes. However, we note that *Okal and Talandier* [1989] reported an M_m measurement of 7.14 at Pasadena, which can reasonably be used at the western U.S. stations (ANMO, JAS, and LON); this leads to Θ^{SS} values of –5.54, –5.58 and –5.59, respectively. While these values would fail to identify the earthquake as truly anomalous, they are indeed in agreement with its character as marginally energy deficient.

Finally, on Figure 8, we similarly test the case of a regular tsunamigenic earthquake, Event 19 (Flores Sea, 1992), to assess the possibility of a false alarm. Individual values of Θ^{SS} are listed at the bottom of Table 3. At all stations, the event is correctly assessed as not slow, with Θ^{SS} ranging from –4.58 (at CTAO) to –5.31 (at AAK). This result is particularly important, because, for all stations considered, M_m systematically overestimates the moment of the earthquake as published by *Dziewonski et al.* [1993]; it can be verified that this is due to the fortuitous distribution of the stations relative to the radiation pattern, rather than to a slow component of the source.

4. Conclusions

1. We have expanded the computation of radiated energy by *Boatwright and Choy*'s [1986] formalism to the case where focal depth and geometry are not known, through the use of the distance-dependent approximation (9) for the generalized radiation coefficient $(F^{sP})^2$.

2. The application of this formalism to a data set of 540 broadband and short-period digital records from 52 earthquakes results in values of the estimated energy E^E in generally good agreement with the NEIC values computed by *Choy and Boatwright* [1995] with the full knowledge of the focal geometry. A notable exception concerns strike-slip earthquakes, for which NEIC values are as much as 1.4 order of magnitude higher than our estimated energies. We attribute this discrepancy to over-correction of the energy flux when using exceedingly small theoretical values of the radiation coefficients and ignoring the scattering of seismic energy outside the geometrical path in the presence of lateral heterogeneity.

3. We define the parameter $\Theta = \log_{10} E^E/M_0$ to characterize the energy-to-moment ratio, as computed from our estimated values. The average value of Θ (–4.98) agrees well both with the value (–4.90) predicted from a combination of theoretical models and scaling relations and with that (–4.80) best fitting the NEIC data set, as reported by *Choy and Boatwright* [1995].

4. While most earthquakes analyzed have Θ in the range –4.5 to –5.6, we find a one-to-one correspondence in our data set between the three recent events independently described in the literature as "tsunami earthquakes" (Nicaragua, Java, Peru) and those having a deficient Θ (by 1 to 1.4 units). This indicates that Θ can be an efficient discriminant of the slow character of these tsunami earthquakes. On the other hand, those tsunamigenic events whose tsunamis can be regarded as normal given the seismological estimate of their size (principally M_0) are characterized by mainstream or higher values of Θ.

With a deficiency of only 0.8 units of Θ, the case of the 1982 Tonga earthquake is less clear-cut, its behavior being intermediate between mainstream events and tsunami earthquakes. This remains in agreement with other seismological properties of this earthquake. Incidentally, it is interesting to speculate at this point on whether the difference in behavior between Events 4 (Tonga) and 18 (Nicaragua) might be related to the different role played by sedimentary structures: lubrication of the fault at depth by subducted sediments in Nicaragua, versus faulting reaching through an accretionary prism (and possibly involving slumping) in Tonga [*Lundgren et al.* 1989; *Kikuchi and Kanamori* [1995].

5. Single-station measurements combining E^E and the mantle magnitude M_m are capable of recognizing the three tsunami earthquakes through single-station parameters Θ^{SS}, which in all cases are found to be less than –5.5, in most cases less than –5.8. Although a large number of technical issues, such as the formal definition and testing of thresholds, are yet to be resolved, these results pave the way for the implementation of automated measurements of E^E, and hence Θ, as part of the

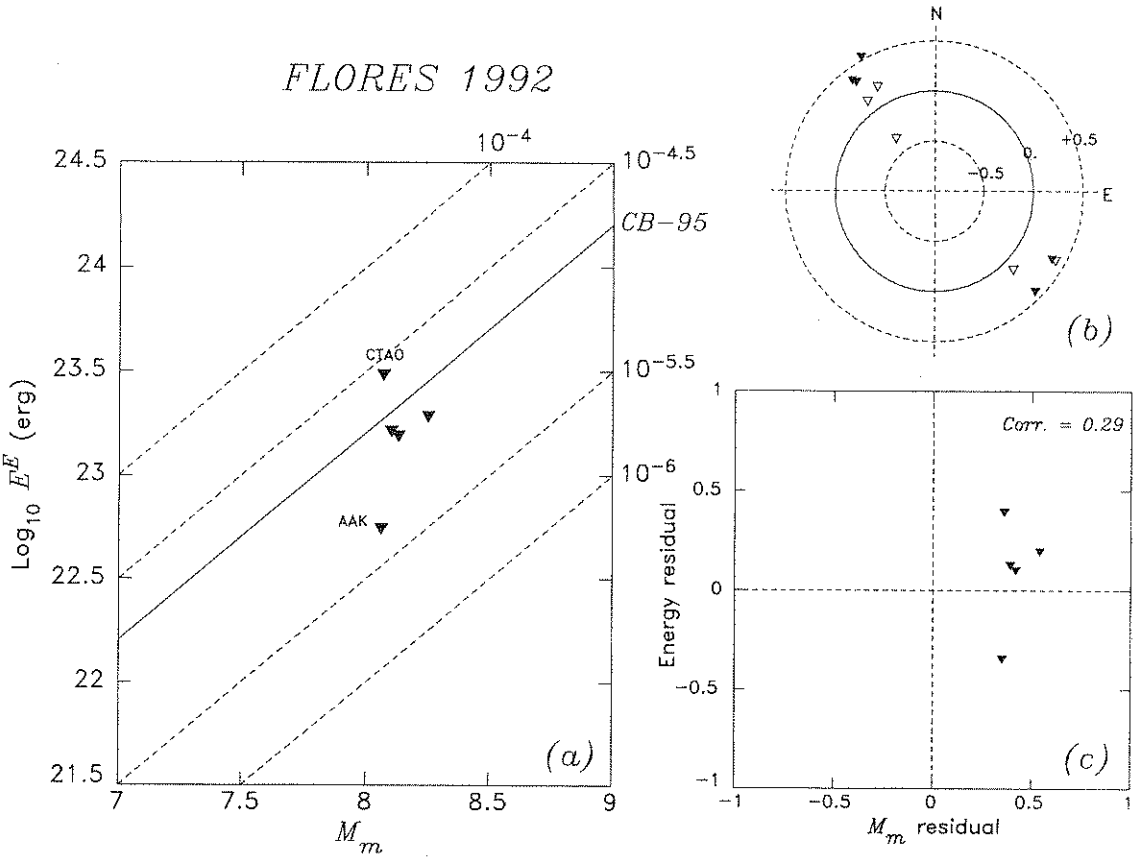

Figure 8. Same as Figure 5 at five stations for the 1992 Flores Sea earthquake (Event 19; not a tsunami earthquake). Note that baselines have been adjusted relative to Figures 5–7.

TREMORS detection and warning algorithm. In order to reap the full societal benefit of this initiative, it will also be necessary to extend the present work to shorter epicentral distances, where accurate tsunami warning is most crucial but where the use of the simple formalism of geometrical ray theory to evaluate body wave amplitudes becomes inappropriate.

Note added in proof (August 12, 1998): The preliminary application of the present formalism to the recent Saundaun, Papua New Guinea, earthquake of July 17, 1998 (Julian Day 198) yields $\Theta = -5.50$, indicating that this event is not anomalously slow, and suggesting that its exceptional tsunami (whose run-up reached 15 m at Sissano Lagoon) may have resulted from underwater slumping.

Acknowledgments. All the data used in this study were obtained from the IRIS consortium. We are grateful to Göran Ekström for access to CMT solutions in advance of formal publication. The paper benefited from careful reviews by Paul Richards, another reviewer, and Associate Editor Greg Beroza. E.A.O. thanks his colleagues in the tsunami community in the United States, France, and Polynesia, for many years of stimulating discussion and collaboration in the field of tsunami warning. This work was supported by the National Science Foundation.

References

Aki, K., and P.G. Richards, *Quantitative Seismology*, 932 pp., W.H. Freeman, New York, 1980.

Boatwright, J., and G.L. Choy, Teleseismic estimates of the energy radiated by shallow earthquakes, *J. Geophys. Res., 91,* 2095-2112, 1986.

Boatwright, J., and J.B. Fletcher, The partition of radiated energy between *P* and *S* waves, *Bull. Seismol. Soc. Am., 74,* 361-376, 1984.

Choy, G.L., and J.L. Boatwright, Global patterns of radiated seismic energy and apparent stress, *J. Geophys. Res., 100,* 18205-18228, 1995.

Courboulex, F., S.K. Singh, J.F. Pacheco, and C.J. Ammon, The 1995 Colima-Jalisco, Mexico, earthquake ($M_w = 8$): A study of the rupture process, *Geophys. Res. Lett., 24,* 1019-1022, 1997.

Der, Z.A., T.W. McElfresh, and A. O'Donnell, An investigation of the regional variation and frequency dependence of attenuation in the United States in the 0.5–4 Hz range, *Geophys. J. Roy. astr. Soc., 69,* 67-100, 1982.

Dziewonski, A.M., A. Friedman, D. Giardini, and J.H. Woodhouse, Global seismicity of 1982: Centroid moment tensor solutions for 308 earthquakes, *Phys. Earth Planet. Inter., 33,* 76-90, 1983.

Dziewonski, A.M., G. Ekström, J.H. Woodhouse, and G. Zwart, Centroid-moment tensor solutions for January-March, 1990, *Phys. Earth Planet. Inter., 65,* 197-206, 1991.

Dziewonski, A.M., G. Ekström, and M.P. Salganik, Centroid-moment tensor solutions for October-December 1992, *Phys. Earth Planet. Inter., 80,* 89-103, 1993.

Dziewonski, A.M., G. Ekström, and M.P. Salganik, Centroid-moment tensor solutions for January-March 1996, *Phys. Earth Planet. Inter., 102,* 1-9, 1997.

Fukao, Y., Tsunami earthquake and subduction processes near deep sea trenches, *J. Geophys. Res., 84,* 2303-2314, 1979.

Geller, R.J., Scaling relations for earthquake source parameters and magnitudes, *Bull. Seismol. Soc. Am., 66,* 1501-1523, 1976.

Guibourg, S., P. Heinrich, and R. Roche, Numerical modeling of the 1995 Chilean tsunami; impact on French Polynesia, *Geophys. Res. Lett., 24,* 775-778, 1997.

Harkrider, D.G., Surface waves in multilayered elastic media, I, Rayleigh and Love waves from buried sources in a multilayered half-space, *Bull. Seismol. Soc. Am., 54,* 627-679, 1964.

Kanamori, H., Mechanism of tsunami earthquakes, *Phys. Earth Planet. Inter., 6,* 346-359, 1972.

Kanamori, H., and D.L. Anderson, Theoretical basis of some empirical relations in seismology, *Bull. Seismol. Soc. Am., 65,* 1073-1095, 1975.

Kanamori, H., and M. Kikuchi, The 1992 Nicaragua earthquake: a slow tsunami earthquake associated with subducted sediment, *Nature, 361,* 714-715, 1993.

Kanamori, H., and G.S. Stewart, Mode of strain release along the Gibbs Fracture Zone, Mid-Atlantic Ridge, *Phys. Earth Planet. Inter., 11,* 312-332, 1976.

Kikuchi, M., and H. Kanamori, Source characteristics of the 1992 Nicaragua tsunami earthquake inferred from teleseismic body waves, *Pure Appl. Geophys., 144,* 441-453, 1995.

Lundgren, P.R., E.A. Okal and D.A. Wiens, Rupture characteristics of the 1982 Tonga and 1986 Kermadec earthquakes, *J. Geophys. Res., 94,* 15521-15539, 1989.

Marshall, P.D., and P.W. Basham, Discrimination between earthquakes and underground explosions employing an improved M_s scale, *Geophys. J. Roy. astr. Soc., 28,* 431-458, 1972.

Okal, E.A., Seismic parameters controlling far-field tsunami amplitudes: A review, *Nat. Hazards, 1,* 67-96, 1988.

Okal, E.A., A student's guide to teleseismic body-wave amplitudes, *Seismol. Res. Lett., 63,* 169-180, 1992.

Okal, E.A., and J. Talandier, M_m: A variable period mantle magnitude, *J. Geophys. Res., 94,* 4169-4193, 1989.

Orowan, E., Mechanism of seismic faulting, *Mem. Geol. Soc. Am., 79,* 323-345, 1960.

Polet, J., and H. Kanamori, The role of sediments in tsunami earthquakes (abstract), *Eos, Trans. AGU, 78,* (46), Fall Mtg. Supp., F627, 1997.

Reymond, D., O. Hyvernaud, and J. Talandier, Automatic detection, location and quantification of earthquakes: Application to tsunami warning, *Pure Appl. Geophys., 135,* 361-382, 1991.

Ruegg, J.-C., et al., The $M_w = 8.1$ Antofagasta (North Chile) earthquake of July 30, 1995: First results from teleseismic and geodetic data, *Geophys. Res. Lett., 23,* 917-920, 1996.

Schindelé, F., D. Reymond, E. Gaucher, and E.A. Okal, Analysis and automatic processing in near-field of the eight 1992-1994 tsunamigenic earthquakes: Improvements in real-time tsunami warning, *Pure Appl. Geophys., 144,* 381–408, 1995.

Scholz, C.H., Scaling laws for large earthquakes: Consequences for physical models, *Bull. Seismol. Soc. Am., 72,* 1-14, 1982.

Talandier, J., and E.A. Okal, An algorithm for automated tsunami warning in French Polynesia, based on mantle magnitudes, *Bull. Seismol. Soc. Am., 79,* 1177-1193, 1989.

Tanioka, Y., and K. Satake, Tsunami generation by horizontal displacement of ocean bottom, *Geophys. Res. Lett., 23,* 861-864, 1996.

Tanioka, Y., L.J. Ruff, and K. Satake, The recent large tsunamigenic earthquakes (abstract), *Eos, Trans. AGU, 77,* (17), Spring Mtg. Supp., S184, 1996.

Tsuji, Y., F. Imamura, H. Matsutomi, C.E. Synolakis, P.T. Nanang, Jumadi, S. Harada, S.S. Han, K. Arai, and B. Cook, Field survey of the East Java earthquake and tsunami of June 3, 1994, *Pure Appl. Geophys., 144,* 839-854, 1995.

Vassiliou, M.S., and H. Kanamori, The energy release in earthquakes, *Bull. Seismol. Soc. Am., 72,* 371-387, 1982.

Wyss, M., Stress estimates for South American shallow and deep earthquakes, *J. Geophys. Res., 78,* 1529-1544, 1970.

A.V. Newman and E.A. Okal, Department of Geological Sciences, Northwestern University, Evanston, IL 60208, USA.

(Received January 12, 1998; revised June 5, 1998;
accepted June 19, 1998.)